

# Hofmeister Effect Mediated Conductivity of Hydrogel Electrolytes for High Performance Supercapacitor

Bingxi Lv,<sup>[a]</sup> Qingqing Guo,<sup>[a]</sup> Xingxiang Ji,<sup>[a]</sup> Ligang Gai,<sup>[a]</sup> and Libin Liu<sup>\*[a]</sup>

Regulating the performance of hydrogel electrolytes by Hofmeister effect has attracted great interest. However, the Hofmeister effects of cations on the conductivity of hydrogel electrolytes are rarely reported. Here, hydrogel electrolytes (polySA) have been fabricated by random copolymerization of zwitterionic monomers in the presence of NH<sub>4</sub>Cl, NaCl and LiCl. The weak interaction between NH<sub>4</sub><sup>+</sup> with water and molecular chains makes polySA-NH<sub>4</sub><sup>+</sup> electrolyte have high conductivity at room temperatures, whereas the strong interaction between Li<sup>+</sup> with water and molecular chains makes polySA-Li<sup>+</sup> electro-

lyte possess good anti-freezing properties and high mechanical strength. The polySA-Li<sup>+</sup> hydrogel electrolyte can have a conductivity of 9.63 mS cm<sup>-1</sup> at -35 °C. Supercapacitors assembled with polySA-Li<sup>+</sup> offers high specific capacitance of 52.25 F g<sup>-1</sup> at 25 °C and 47.75 F g<sup>-1</sup> at -35 °C. The capacitance retention is 94.64% after 10 days at -35 °C. Our work shows that different properties of hydrogel electrolytes can be achieved by regulating Hofmeister effect, which provides a new way to prepare high-performance energy storage materials.

## 1. Introduction

In recent years, hydrogel electrolytes have become a hot research topic due to their unique structure rich in large amounts of water, which have high ionic conductivity, excellent safety, and adjustable mechanical properties.<sup>[1-4]</sup> Hydrogel electrolytes are generally divided into acid electrolytes, alkaline electrolytes and neutral electrolytes according to their acid-base properties. Acidic or alkaline electrolytes, which are enriched with H<sup>+</sup><sup>[5-8]</sup> or OH<sup>-</sup><sup>[9-12]</sup> respectively, and have been studied and applied due to their extremely low hydration radius and ultra-high conductivity. For example, Sun<sup>[8]</sup> used only 1 M sulfuric acid to prepare a hydrogel electrolyte of 210 mS cm<sup>-1</sup> at 25 °C. Zhang<sup>[12]</sup> obtained the hydrogel electrolyte by soaking in a mixed solution of KOH and KI and a high conductivity of 223 mS m<sup>-1</sup> at 20 °C was achieved. Although acidic or alkaline hydrogel electrolytes have been widely reported, the corrosiveness of acids and alkalis has always been a thorny issue. As an alternative solution, salts (such as LiCl, NaCl, etc.) are generally neutral and are one of the most suitable options to balance electrochemical performance and safety of hydrogel electrolyte.<sup>[13-17]</sup> However, there are many types of salt ions, and the hydration ion radii of each type of salt ion are different. The interaction between ions and water molecules or polymer molecular chains will affect the conductivity and mechanical properties of hydrogel electrolytes, and then affect the performance of energy storage devices. How to achieve high-performance energy storage devices by selecting or modulating differ-

ent salt ions in a specific scenario is gradually becoming complex and cumbersome.

In order to solve the above issues, the outstanding work of our predecessors has provided us with reference. In 1888, Dutch scientist Hofmeister discovered that different salts exhibit different abilities to precipitate proteins from aqueous solutions, which is known as the Hofmeister effect or ion-specific effect.<sup>[18,19]</sup> This effect is mainly reflected in two types of interactions.<sup>[20-25]</sup> One is to describe the capacity of a particular ion to "make" or "break" water structure, and the other is to describe the interactions between ions and molecular chains. Previous literatures have focused on the study of the Hofmeister effect on the solubility of macromolecules<sup>[20,21,23]</sup> or the mechanical properties of the hydrogel systems.<sup>[26-30]</sup> For example, Wu<sup>[29]</sup> et al. designed hydrogels with different mechanical properties by tuning the aggregation of the hydrophilic polymer chains at molecular level via the Hofmeister effect. Recently, this effect has also been extended to electrolyte systems.<sup>[13,31-35]</sup> By regulating the Hofmeister effect, water activity, solvation structures and electrochemical window have been studied in these electrolytes. However, these reports mostly focus on the effect of anions on the electrolytes. The influence of cations on the conductive hydrogel is only reflected in the regulation of mechanical properties,<sup>[36]</sup> while the influence on the conductivity is not involved. Therefore, the study of the synergistic effect of cations with water and molecular chains on the conductivity of the hydrogel electrolyte, especially at low temperature is highly demanded.

In this work, we studied the interaction between cations and water molecules as well as polymer chains in the hydrogel electrolytes which were fabricated by one-step radical polymerization of 2-acrylamido-2-methyl-1-propanesulfonic acid sodium salt solution (AMPS-Na) and zwitterionic [(methacryloyloxy)ethyl]dimethyl-(3-sulfopropyl)ammonium hydroxide (SBMA) in the presence of different salts (Figure 1). N, N-methylenebisacrylamide (MBA) was used as a cross-linker. In

[a] B. Lv, Q. Guo, X. Ji, L. Gai, L. Liu

School of Chemistry and Chemical Engineering, State Key Laboratory of Biobased Material and Green Papermaking, Qilu University of Technology (Shandong Academy of Sciences), Jinan 250353, P. R. China

E-mail: lbliu@qlu.edu.cn

 Supporting information for this article is available on the WWW under <https://doi.org/10.1002/batt.202400245>

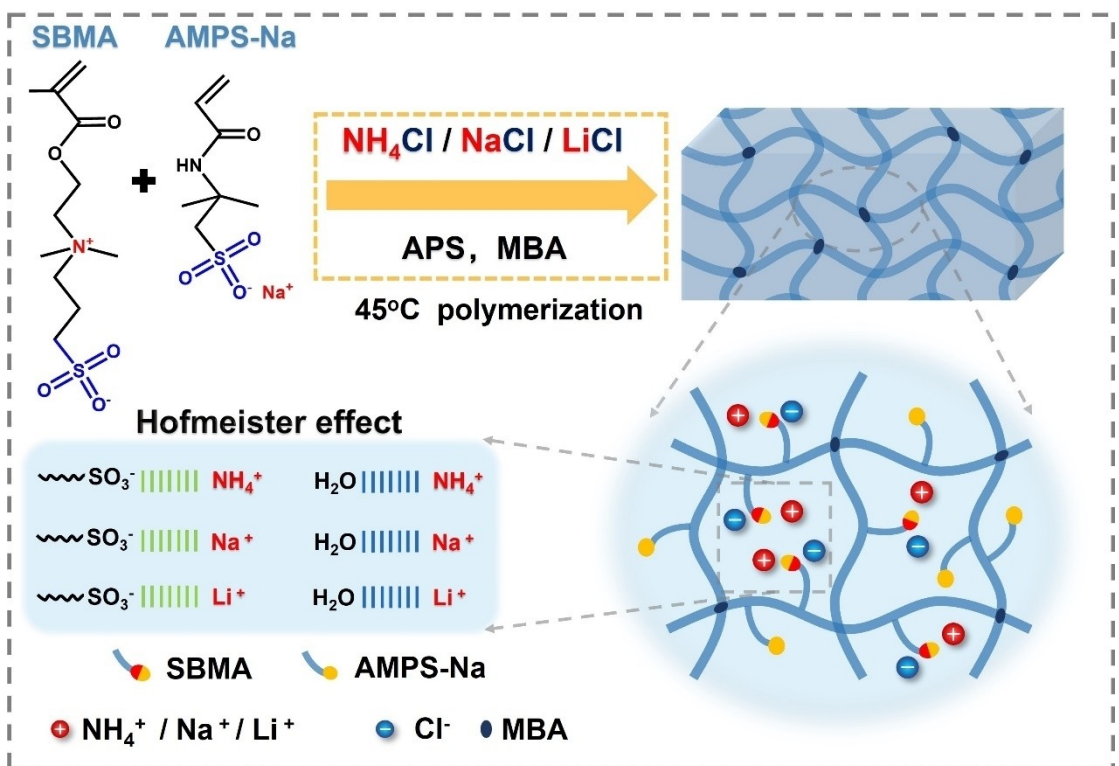


Figure 1. Schematic diagram of the fabrication process of hydrogel electrolytes and the Hofmeister effect in the electrolytes.

order to compare the influence of different cations, anion of Cl<sup>-</sup> was fixed and cations of NH<sub>4</sub><sup>+</sup>, Na<sup>+</sup>, Li<sup>+</sup> were selected. The weaker interaction between NH<sub>4</sub><sup>+</sup> with water and molecular chains makes it easier for NH<sub>4</sub><sup>+</sup> to migrate in the hydrogel, which can provide better electrical conductivity for the hydrogel electrolyte at room temperature. The strong interaction between Li<sup>+</sup> with water and molecular chains, not only gives the hydrogel electrolyte stronger mechanical properties, but also gives the hydrogel electrolyte better freezing resistance and water retention by destroying more hydrogen bonds of water. Supercapacitors (SC) assembled with polySA-Li<sup>+</sup> electrolyte offers high specific capacitance of 52.25 F g<sup>-1</sup> at 25 °C and 47.75 F g<sup>-1</sup> at -35 °C. The capacitance retention is 94.64% after 10 days at -35 °C.

## 2. Results and Discussion

In the previous work, ionic polymer chains have been reported to facilitate ion transport.<sup>[37–39]</sup> Here, the ionic monomers of SBMA and AMPS-Na were selected to study the Hofmeister effect. The resulted hydrogel electrolyte was abbreviated as polySA-M, where S is the monomer of SBMA, A is the monomer of AMPS-Na, M is the cation: NH<sub>4</sub><sup>+</sup>, Na<sup>+</sup>, Li<sup>+</sup>, respectively. The hydrogel prepared in the same way without adding salts was abbreviated as polySA-H<sub>2</sub>O. First, we measured the conductivity of hydrogel electrolytes synthesized with different monomer ratios at the same salt concentration. It is found that the monomer ratio has almost no effect on the conductivity

(Figure S1). Thus, the monomer ratio of 1:1 between SBMA and AMPS-Na was chosen for the next study.

Next, the conductivities of hydrogel electrolytes with different salt concentrations at 25 °C were measured. The concentration was ranged from 0.3 to 5 mol L<sup>-1</sup>. As shown in Figure 2a, the conductivities of all hydrogel electrolytes increase with increasing salts concentration. At the same concentration, the conductivity of polySA-Na<sup>+</sup> and polySA-Li<sup>+</sup> is not significantly different, while the conductivity of polySA-NH<sub>4</sub><sup>+</sup> is highest. This indicates that NH<sub>4</sub><sup>+</sup> is beneficial for the conductivity of the hydrogel electrolyte. At different temperatures range of 0~40 °C, the conductivity of NH<sub>4</sub><sup>+</sup> has always been superior to the conductivity of the other two ions (Figure 2b). In addition, the ionic conductivity in the measured temperature range is linear with the reciprocal absolute temperature, indicating that the conductivity of the electrolyte obeys Arrhenius' law.<sup>[40]</sup> The polySA-NH<sub>4</sub><sup>+</sup> has the lowest activation energy ( $E_a$ ) of 9.92 kJ mol<sup>-1</sup> compared to polySA-Na<sup>+</sup> and polySA-Li<sup>+</sup>. The  $E_a$  represents the energy barrier that ion migration must overcome. The smaller the  $E_a$  is, the easier the ion migration is.<sup>[41]</sup> The high ionic conductivity of polySA-NH<sub>4</sub><sup>+</sup> may be due to the jump migration of NH<sub>4</sub><sup>+</sup> at the sulfonic acid groups of the polymer chain, similar to the migration mechanism of metal ions in amphotolytic electrolytes.<sup>[42–44]</sup> To further understand the interactions between the ionic groups of the polymer chains and the salt ions, Raman spectroscopy was performed on the hydrogel electrolytes. As shown in Figure 2c, the  $\text{--CH}_3$  stretching vibration of  $\text{--N}^+(\text{CH}_3)_2$  changes for all polySA-M electrolytes due to the interaction of Cl<sup>-</sup> after addition of salts

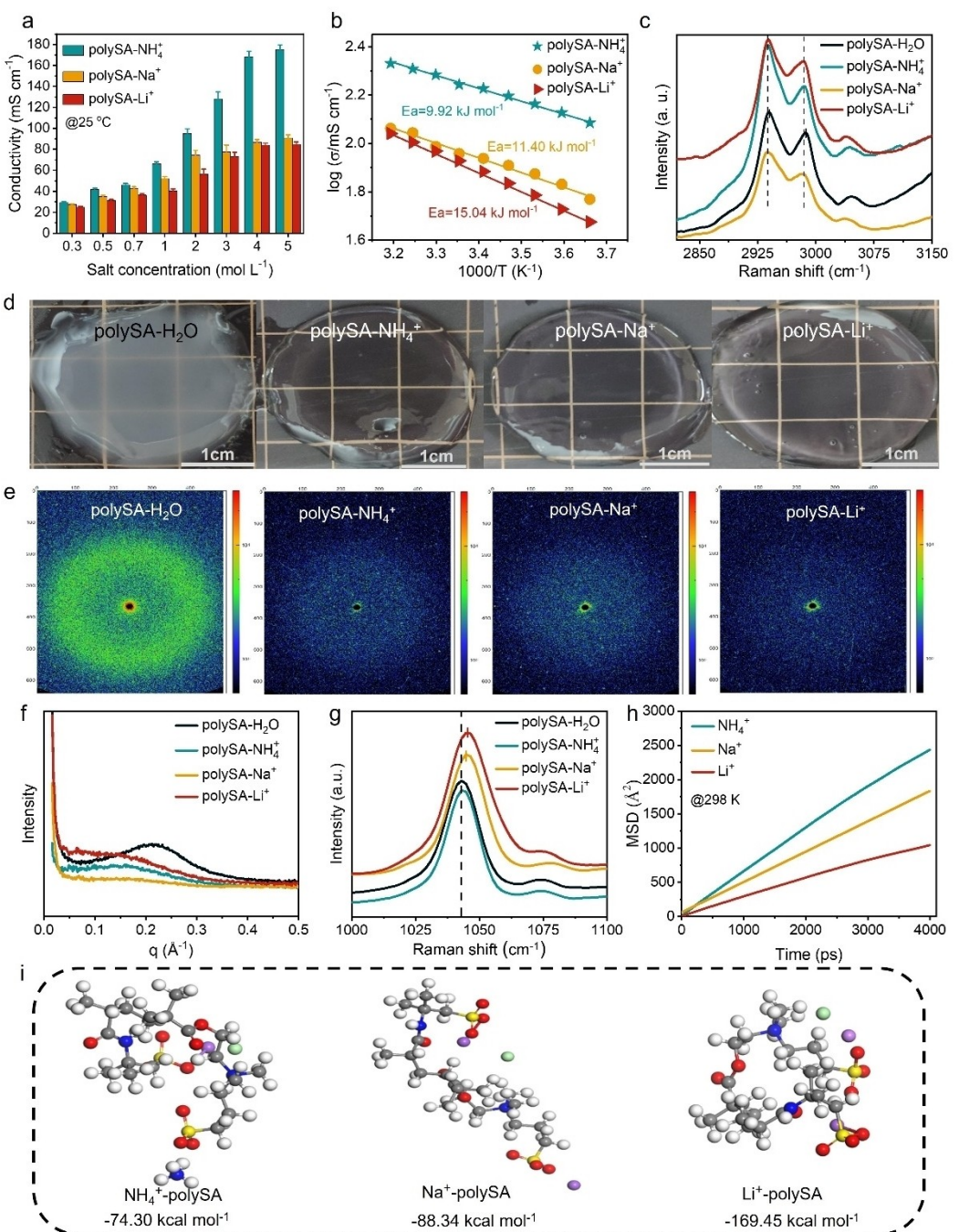


**Figure 2.** a) Conductivity of three kinds of salts-based hydrogel electrolytes with different salts concentrations. b) Temperature dependence of ionic conductivity of the hydrogel electrolytes. c) Raman spectra of  $-\text{N}^+(\text{CH}_3)_2$  for hydrogels with or without salts. d) Photograph images of hydrogels with or without salts. e) 2 D pattern and f) SAXS spectra of hydrogels with or without salts. g) Raman spectra of  $-\text{SO}_3^-$ . h) MSD of the cations in the hydrogel electrolytes at 298 K. i) Binding energy of cations with the polymer chains in the hydrogel electrolytes at 298 K.

compared with that of pure hydrogels, indicating that the electrostatic equilibrium of anionic groups and cationic groups in the hydrogels was disrupted. The addition of salt makes the hydrogel present a transparent state (Figure 2d), which also means that the aggregation of molecular chains is disrupted and the molecular chains stretch out. Small-angle x-ray scattering (SAXS) tests further confirm that there is no phase separation in the polySA-M electrolytes. As shown in Figure 2e

and f, an obvious diffraction circle and wide peak appear in pure hydrogels, whereas no peaks or diffraction circles are observed in the polySA-M electrolytes. Different cations ( $\text{NH}_4^+$ ,  $\text{Na}^+$ ,  $\text{Li}^+$ ) will interact with sulfonic acid groups in the polymer chains. As shown in the Raman of Figure 2g, the S=O stretching vibrational peaks of polySA- $\text{Na}^+$  and polySA- $\text{Li}^+$  are shifted to  $1044 \text{ cm}^{-1}$  and  $1046 \text{ cm}^{-1}$ , respectively, whereas the S=O stretching vibrational peaks of polySA- $\text{NH}_4^+$  are essentially the

same as that of the pure water hydrogel ( $1042\text{ cm}^{-1}$ ), indicating that the interaction between  $\text{NH}_4^+$  and  $\text{SO}_3^-$  is weaker than that between  $\text{Na}^+/\text{Li}^+$  and  $\text{SO}_3^-$ . The results of infrared spectra are consistent with those of Raman spectra (Figure S2). Although the sulfonic acid groups on the polymer chains provide channels for the transport of conductive ions, the weak electrostatic interactions between conductive ions and the polymer chain may be more favorable for ion transport. The root mean square ion displacement (MSD) simulation was further carried out to prove the ionic diffusion rate (Figure S3). As shown in Figure 2h, the displacement and time interval of the three cations in the electrolytes present linear relationships. The higher the slope of the curve is, the faster the diffusion rate of ions is. This is consistent with the measured order of conductivity. The binding energy between the polymer chains and the binding energy between salt ions and polymer chains were calculated by density functional theory (DFT). As shown in Figure 2i and Figure S4, after addition of salt, polySA- $\text{NH}_4^+$  electrolyte shows a lower binding energy of  $-74.30\text{ kcal mol}^{-1}$  compared to polySA- $\text{Na}^+$  electrolyte ( $-88.33\text{ kcal mol}^{-1}$ ) and polySA- $\text{Li}^+$  electrolyte ( $-169.45\text{ kcal mol}^{-1}$ ), indicating that weak electrostatic interactions are more conducive to ion transport.

In addition, the addition of salt also leads to changes in the mechanical properties of the hydrogel. The storage modulus  $G'$  of the all polySA-M electrolytes is larger than the loss modulus  $G''$  indicating the solid-state behavior. PolySA- $\text{NH}_4^+$  electrolyte exhibits the lowest  $G'$  compared to polySA- $\text{Na}^+$  and polySA- $\text{Li}^+$  electrolytes (Figure S5). The complex viscosity usually indicates the internal resistance of the materials. As shown in Figure 3a, the complex viscosity of polySA- $\text{Na}^+$  and polySA- $\text{Li}^+$  hydrogel electrolytes are higher than that of polySA- $\text{NH}_4^+$  hydrogel electrolyte, which indicates that the conductive ions are more

favorable to migrate in low viscosity polySA- $\text{NH}_4^+$  electrolyte. The stress-strain curves have been shown in Figure S6. The polySA- $\text{Li}^+$  hydrogel electrolytes have higher mechanical strength compared to other hydrogel electrolytes, which is consistent with the results of viscosity.

The conductivity of different polySA-M electrolytes is reflected in the Hofmeister effect not only between cations and molecular chains, but also between cations and water molecules. To confirm the state of water, low-field nuclear magnetic resonance (LF-NMR) test was performed, which mainly reflects the mobility of water molecules by measuring the relaxation time and helps to understand the binding of water. The time regions in the range of  $\sim 10\text{ ms}$  and  $\sim 1000\text{ ms}$  belong to bound water and free water, respectively. The shorter the relaxation time is, the stronger the bonding of water to material is.<sup>[45,46]</sup> As shown in Figure 3b, the pure water hydrogel has the longest relaxation time, which is attributed to the absence of salt ions in the pure water hydrogel and the weak binding of water only to the polymer chains. In contrast, the relaxation time of polySA- $\text{Li}^+$  is shorter than that of polySA- $\text{Na}^+$  and polySA- $\text{NH}_4^+$ , suggesting that  $\text{Li}^+$  is able to bind more water molecules than  $\text{Na}^+$  and  $\text{NH}_4^+$ . The binding ability of metal ions with  $\text{H}_2\text{O}$  is also in agreement with the radius of the hydrated ions, where the hydrated ionic radius of  $\text{Li}^+$  is larger than that of  $\text{Na}^+$  and  $\text{NH}_4^+$ .<sup>[47]</sup> The strong binding ability of  $\text{Li}^+$  with  $\text{H}_2\text{O}$  is also reflected in the strong water retention ability of hydrogel electrolyte. The polySA- $\text{Li}^+$  hydrogel electrolyte can retain 64 wt% water contents after 18 hours exposed at  $25^\circ\text{C}$  and 45% relative humidity conditions, much higher than other hydrogel electrolytes (Figure 3c). The diffusion coefficient of water molecules in the electrolyte further indicates the binding ability of water molecules with metal ions. The diffusion coefficient of water molecules is calculated according to MSD.

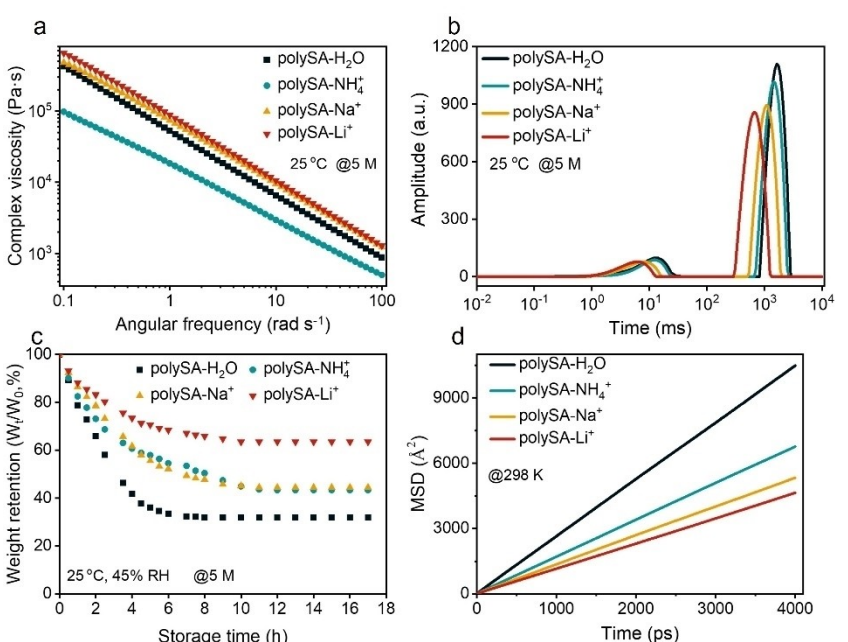


**Figure 3.** a) Complex viscosity of the hydrogels with and without salts. b) LF-NMR of the hydrogels with and without salts. c) Weight retention rate of the hydrogels with and without salts. d) MSD of water molecules in the hydrogels at 298 K.

As shown in Figure 3d, the polySA-Li<sup>+</sup> exhibits the lowest diffusion coefficient of water molecular ( $1.93 \times 10^{-5} \text{ cm}^2 \text{s}^{-1}$ ) compared to polySA-Na<sup>+</sup> ( $2.22 \times 10^{-5} \text{ cm}^2 \text{s}^{-1}$ ) and polySA-NH<sub>4</sub><sup>+</sup> ( $2.82 \times 10^{-5} \text{ cm}^2 \text{s}^{-1}$ ). The strong binding ability of water to Li<sup>+</sup> restricts the movement of water and also makes the polySA-Li<sup>+</sup> electrolyte possess good anti-freezing ability.

The conductivity of hydrogel electrolytes at subzero temperatures is also affected by Hofmeister effect. As shown in Figure 4a, polySA-NH<sub>4</sub><sup>+</sup> hydrogel electrolyte and polySA-Na<sup>+</sup> hydrogel electrolyte almost lose conductivity at  $-15^\circ\text{C}$  and  $-25^\circ\text{C}$  respectively, while the polySA-Li<sup>+</sup> hydrogel electrolyte can still have a conductivity of  $9.63 \text{ mScm}^{-1}$  at  $-35^\circ\text{C}$ . Differential scanning calorimetry (DSC) is used to observe the effect of different cationic on the freezing point of the hydrogel electrolytes. As shown in Figure 4b, pure water hydrogel has a freezing point of  $0.8^\circ\text{C}$  due to the absence of antifreezing agents. The freezing point of polySA-NH<sub>4</sub><sup>+</sup> and polySA-Na<sup>+</sup> is  $-13.9^\circ\text{C}$  and  $-18.6^\circ\text{C}$ , respectively. The endothermic peak of polySA-Li<sup>+</sup> is not observed in the DSC curves, indicating that there is no change in heat flow in the electrolyte. The photographs of the cooling process indicate that, pure water hydrogel, polySA-NH<sub>4</sub><sup>+</sup> and polySA-Na<sup>+</sup> harden and whiten at  $0^\circ\text{C}$ ,  $-15^\circ\text{C}$ , and  $-25^\circ\text{C}$ , respectively (Figure 4c). The polySA-Li<sup>+</sup> remains transparent within the measured temperature range. To further understand the inner structure of the electrolytes at low temperature, temperature sweep of rheology was performed. As shown in Figure 4d, the G' of pure water

hydrogel, polySA-NH<sub>4</sub><sup>+</sup> and polySA-Na<sup>+</sup> sharply increases at about  $0^\circ\text{C}$ ,  $-13^\circ\text{C}$  and  $-20^\circ\text{C}$ , respectively, indicating the freeze of electrolyte. The freezing of polySA-Li<sup>+</sup> occurs at around  $-40^\circ\text{C}$ , demonstrating that the strong interaction between Li<sup>+</sup> and water prevents water molecules from freezing and allows the hydrogel electrolyte to maintain conductivity at low temperatures.

The interactions between metal ions and water molecules were demonstrated by Raman spectroscopy. As shown in Figure 5a, a wide peak of the  $\text{--OH}$  stretching vibration belonging to water molecules ( $3000\text{--}3700 \text{ cm}^{-1}$ ) are observed. The main peak at  $3432 \text{ cm}^{-1}$  for pure hydrogel was blue shifted to  $3437 \text{ cm}^{-1}$ ,  $3442 \text{ cm}^{-1}$ , and  $3443 \text{ cm}^{-1}$  for polySA-NH<sub>4</sub><sup>+</sup>, polySA-Na<sup>+</sup>, polySA-Li<sup>+</sup>, indicating that the addition of salt disrupts the hydrogen-bonding network between water molecules. According to the previous reports,<sup>[48,49]</sup> the stretching vibration can be divided into three main peaks at  $\sim 3230$ ,  $\sim 3450$ , and  $\sim 3620 \text{ cm}^{-1}$  corresponding to strong hydrogen bonds (H-bonds), weak H-bonds and non-H-bonds (Figure 5b). The content of strong H-bonded water for different polySA-M electrolytes was calculated by the area of the fitted peaks. Compared to polySA-Na<sup>+</sup> and polySA-NH<sub>4</sub><sup>+</sup> electrolytes, polySA-Li<sup>+</sup> has the least amount of strong H-bonded water (Figure 5c, Figure S7), indicating that the interaction between Li<sup>+</sup> and water is stronger than that between NH<sub>4</sub><sup>+</sup>/Na<sup>+</sup> and water. The DFT calculation also reveals that Li<sup>+</sup> has a stronger interaction with water ( $-23.44 \text{ kcal mol}^{-1}$ ) compared to Na<sup>+</sup>

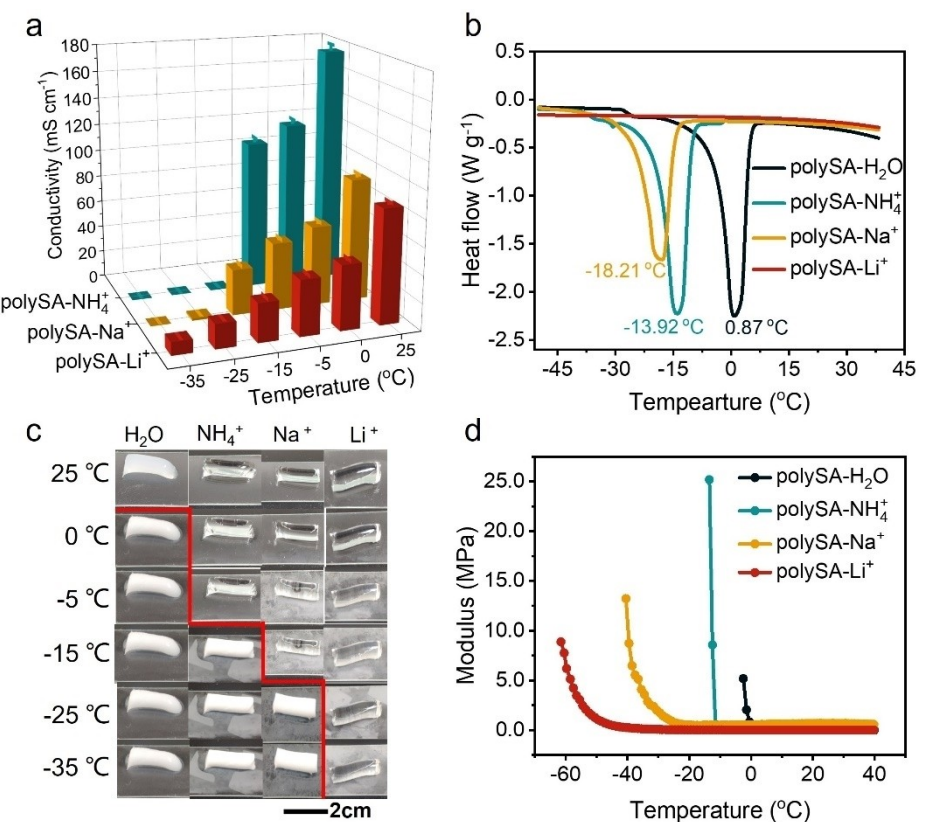


**Figure 4.** a) Low-temperature conductivity of polySA-M hydrogel electrolytes. b) DSC curves of pure hydrogel and polySA-M hydrogel electrolytes. c) Photographs of all hydrogels at different temperatures. d) Low-temperature rheology of pure hydrogel and polySA-M hydrogel electrolytes.

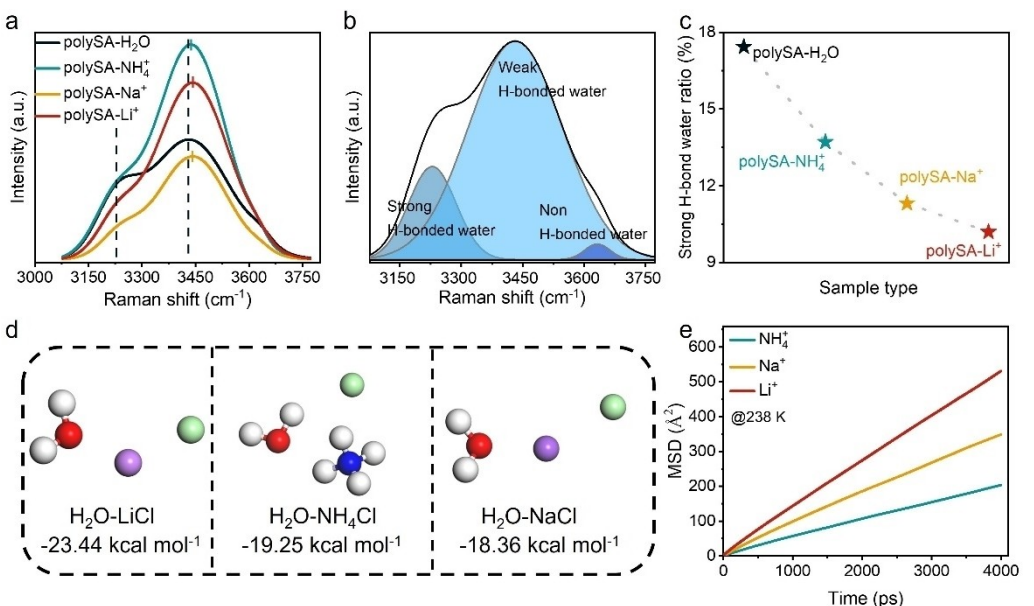


**Figure 5.** a) Raman spectra of –OH stretching vibration. b) Fitted O–H stretching vibration representing water molecules with strong, weak and non-hydrogen bonds (H-bonds). c) Ratio of strong H-bonded water for different hydrogels. d) Binding energy of H<sub>2</sub>O with different metal ions. e) MSD of cations in polySA–M hydrogel electrolytes at 238 K.

( $-18.36 \text{ kcal mol}^{-1}$ ) and  $\text{NH}_4^+$  ( $-19.25 \text{ kcal mol}^{-1}$ ) (Figure 5d). The strong binding ability of water to  $\text{Li}^+$  makes polySA- $\text{Li}^+$  electrolyte possess good anti-freezing ability and high conductivity at subzero temperature. To further confirm this, the diffusion speed of different cations in the hydrogel electrolyte was simulated by MSD at 238 K ( $-35^\circ\text{C}$ ) (Figure S8). As shown in Figure 5e, the  $\text{Li}^+$  exhibits the highest diffusion coefficient ( $2.21 \times 10^{-6} \text{ cm}^2 \text{s}^{-1}$ ) compared to  $\text{Na}^+$  ( $1.45 \times 10^{-6} \text{ cm}^2 \text{s}^{-1}$ ) and  $\text{NH}_4^+$  ( $0.85 \times 10^{-6} \text{ cm}^2 \text{s}^{-1}$ ), which is consistent with the measured conductivity of the electrolytes at subzero temperature (Figure 4a).

Considering the low-temperature anti-freezing performance and conductivity, polySA- $\text{Li}^+$  was used to assemble “sandwich” type supercapacitors (SCs) (Figure 6a). To ensure the long-term application of the electrolyte, the recovery ability and durability of polySA- $\text{Li}^+$  was measured by rheological methods. As shown in Figure 6b, the strain was maintained at 100% oscillation state for 100 s and then immediately returned to 1% strain, after 8000 cycles  $G'$  and  $G''$  quickly returned to their original values. Even if the strain was maintained at 200%, 300%, and 400% for 100 s alternatively,  $G'$  and  $G''$  still returned to the original value (Figure 6c). Then, the electrochemical performance of polySA- $\text{Li}^+$  assembled supercapacitor was measured. The voltage window of the SC was first tested at a scan speed of  $100 \text{ mV s}^{-1}$ . As shown in Figure 6d, at the electrochemical window of  $0.8 \text{ V}$ , the cyclic voltammetry (CV) curve of the SC shows a nearly rectangular shape, so the voltage window is fixed at  $0.8 \text{ V}$  for the subsequent test. At a scan speed from  $50$  to  $500 \text{ mV s}^{-1}$ , the CV curves show rectangular shapes and have only slight deformation at  $1000 \text{ mV s}^{-1}$ . The galvanostatic charge-discharge (GCD) tests present a standard inverted triangle shape with almost no voltage drop at current densities from  $50$  to  $1000 \text{ mA g}^{-1}$ . These results all indicate that the SC exhibits good

electric double layer capacitance behavior at room temperature. The cyclic stability of the SC is also an important indicator. When the SC is charged and discharged 8000 cycles at a current density of  $0.5 \text{ A g}^{-1}$ , the CV curves and the GCD curves of SC only change slightly compared with the initial state (Figure S9). The specific capacitance retention can reach 92%, and the coulombic efficiency can basically be maintained at around 100% (Figure 6g). These tests show that the SC have good cycle stability. In practical applications, connecting multiple SCs. in parallel or in series can achieve higher voltage and energy density. In our work, compared with a single SC, two SCs in series show two times the electrochemical window in both CV and GCD tests, and the current density of two parallel SCs increases to twice that of a single SC (Figure 6h-i).

In addition, we also tested the SC performance at subzero temperature. As shown in Figure 7a, the CV curves change from rectangle shape to deformed rectangle shape as the temperature decreases from  $25$  to  $-35^\circ\text{C}$ . The GCD curves at different temperatures show the almost triangle shapes (Figure 7b). The electrochemical impedance spectroscopy (EIS) at different temperatures shows that the resistance of SC increases from  $4.7 \Omega$  at  $25^\circ\text{C}$  to  $14.8 \Omega$  at  $-35^\circ\text{C}$  (Figure 7c). In the low-frequency region, the curve is almost perpendicular to the X axis, which reflects the fast ion diffusion behavior in the polySA- $\text{Li}^+$  electrolyte. At  $-35^\circ\text{C}$ , the SC still shows good electrochemical performance as confirmed by CV (Figure 7d) and GCD curves (Figure 7e). The capacitance of SC during the cooling process is shown in Figure S10. The mass specific capacitance at  $-35^\circ\text{C}$  is  $40.1 \text{ F g}^{-1}$ , which is 80.5% of that at  $25^\circ\text{C}$  ( $49.8 \text{ F g}^{-1}$ ), indicating the good electrical behavior. Even at a high current density of  $1000 \text{ mA g}^{-1}$ , the capacitance of SC can still maintain 64% of that at  $25^\circ\text{C}$  (Figure 7f). Our SC also has good cycle stability. At after 8000 cycles at  $-35^\circ\text{C}$ , the CV curves and GCD

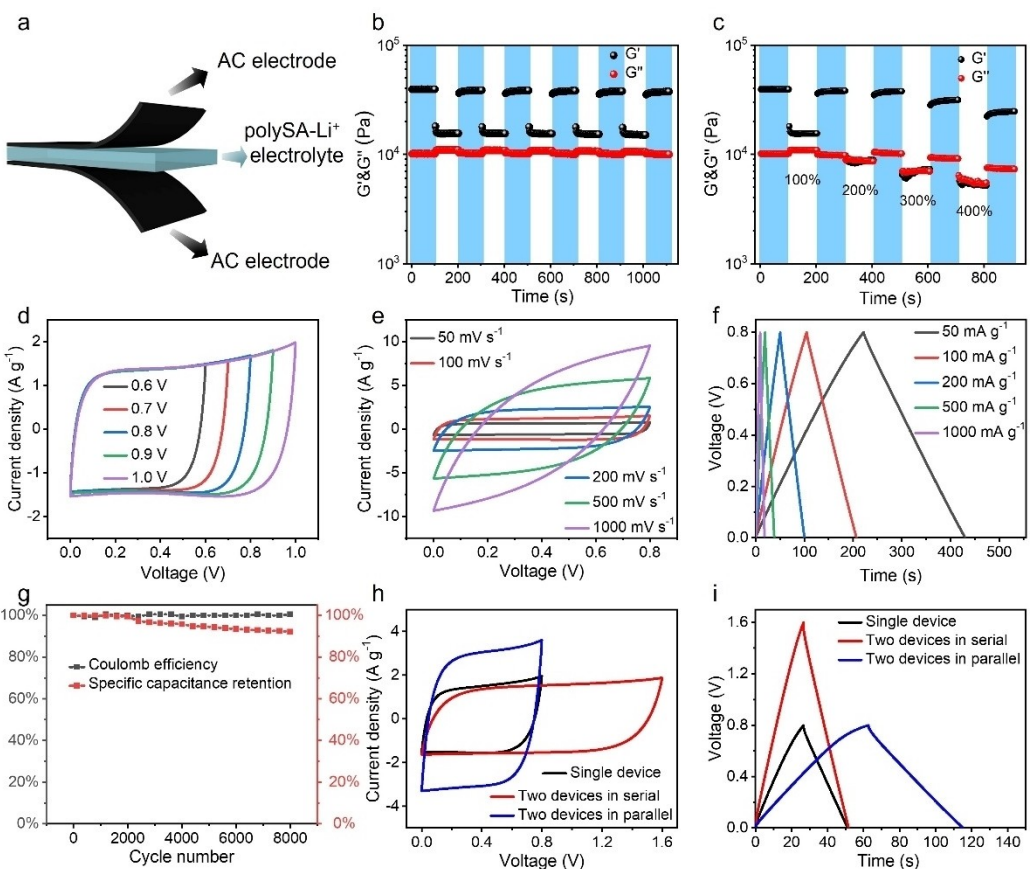


**Figure 6.** a) The diagram of the polySA-Li<sup>+</sup> electrolyte assembled SC. b) G' and G'' of polySA-Li<sup>+</sup> electrolyte under alternate strain of 1 and 100%, respectively. c) G' and G'' of polySA-Li<sup>+</sup> electrolyte under alternate strain of 1, 100, 200, 300 and 400%, respectively. d) CV curves at different voltage window. e) CV curves at different scan speeds. f) GCD curves at different current densities. g) Coulombic efficiency and specific capacitance retention of SC at room temperature after 8000 cycles. h and i) CV and GCD curves of two SCs connected in series and parallel.

curves of SC has only slight changes compared with the initial state (Figure S11). The specific capacitance retention rate of SC can reach 98% (Figure 7g). Even after 10 freezing-thawing cycles, the capacitance of the SC is still the same as that at room temperature (Figure 7h). In addition, when the SC was placed at -35 °C for 10 days, the capacitance only reduced to 95% of its original one (Figure 7i). The performance of the preferred SC has been compared with that reported in literatures. As shown in Table S1, the frost resistance and low temperature cycle stability of our SC is at the highest level compared to that of other hydrogel electrolyte assembled SC. The above data fully demonstrate that the SC assembled with polySA-Li<sup>+</sup> hydrogel electrolyte has good electrochemical performance at low temperatures.

### 3. Conclusions

In short, in order to study the Hofmeister effect of cations on hydrogel electrolytes in terms of conductivity and freezing resistance, we have fabricated ionic hydrogel electrolytes in the presence of different salt ions. The interaction between cations and molecular chains was studied by Raman, SAXS and rheology tests. The weak interaction between NH<sub>4</sub><sup>+</sup> and the

polymer is beneficial to NH<sub>4</sub><sup>+</sup> migration. The strong interaction between Li<sup>+</sup> and the polymer chains is beneficial to higher mechanical properties of hydrogels. The interaction between cations and water was studied by LF-NMR and MSD. The strong interaction between Li<sup>+</sup> and water is beneficial to better freezing resistance and water retention of hydrogels. Supercapacitor assembled with polySA-Li<sup>+</sup> electrolyte offers high specific capacitance of 52.25 F g<sup>-1</sup> at 25 °C and 47.75 F g<sup>-1</sup> at -35 °C. The capacitance retention is 94.64% after 10 days at -35 °C. Our work provides a reference for selecting suitable salt ions for hydrogel electrolytes with different properties.

### Supporting Information Summary

Supporting Information is available free of charge at DOI. Experimental Section and Characterization, Figure S1–S11, Table S1.

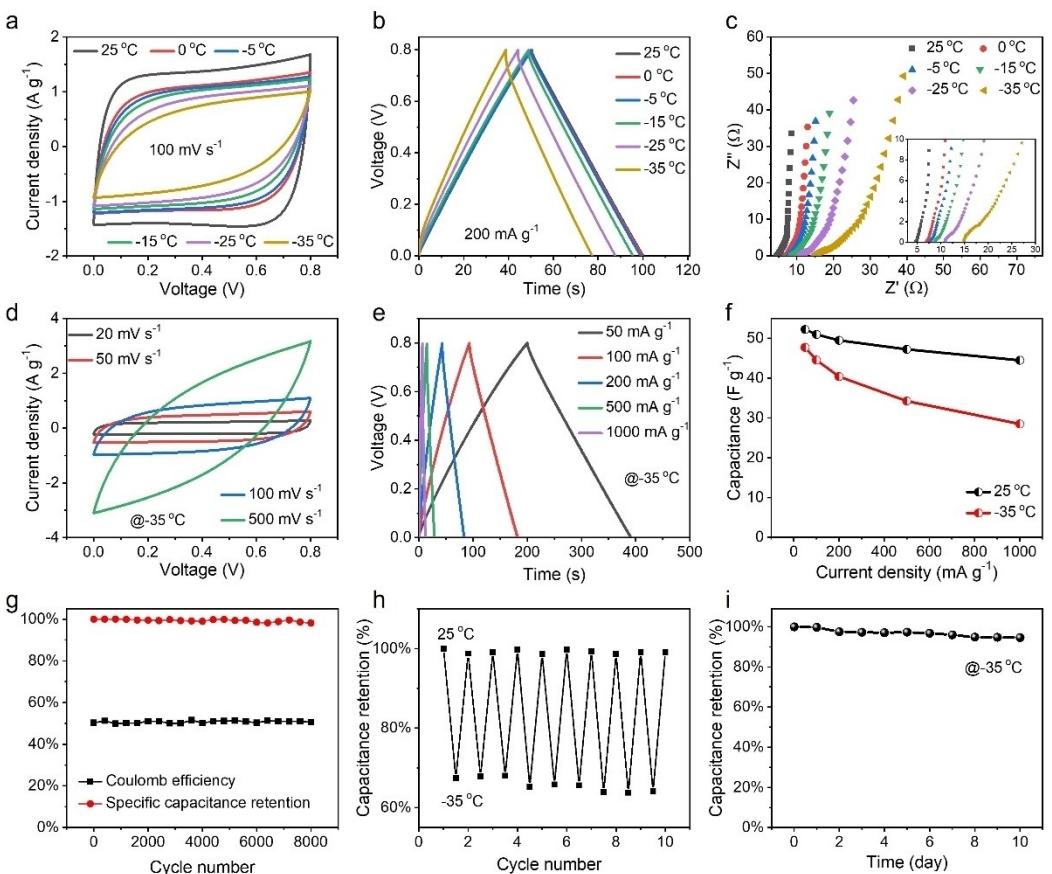


**Figure 7.** a) CV, b) GCD and c) EIS of SC at different temperatures. d) CV curves of the SC at different scan speeds at  $-35^{\circ}\text{C}$ . e) GCD curves of the SC at different current densities at  $-35^{\circ}\text{C}$ . f) Capacitance of the SC at different current densities at  $25^{\circ}\text{C}$  and  $-35^{\circ}\text{C}$ . g) Coulombic efficiency and specific capacitance retention of SC after 8000 cycles at  $-35^{\circ}\text{C}$ . h) Capacitance retention of SC after 10 cycles at  $25^{\circ}\text{C}$  and  $-35^{\circ}\text{C}$  alternatively. i) Capacitance retention of SC stored at  $-35^{\circ}\text{C}$  for 10 days.

## Acknowledgements

We acknowledge the support from the National Natural Science Foundation of China (52173256), Taishan Scholars Program and Jinan Innovation Team(202228021).

## Conflict of Interests

The authors declare no competing interests.

## Data Availability Statement

The data that support the findings of this study are available from the corresponding author upon reasonable request.

**Keywords:** Anti-freeze · Hofmeister effect · Conductivity · Hydrogel electrolyte · Supercapacitor

[1] X. Liu, D. Wu, H. Wang, Q. Wang, *Adv Mater* **2014**, 26(25), 4370–5.

- [2] D. P. Dubal, N. R. Chodankar, D. H. Kim, P. Gomez-Romero, *Chem Soc Rev* **2018**, 47(6), 2065–2129.
- [3] X. Hou, T. P. Pollard, X. He, L. Du, X. Ju, W. Zhao, M. Li, J. Wang, *Adv. Energy Mater.* **2022**, 12(23), 2200401.
- [4] X. Lu, M. Yu, G. Wang, Y. Tong, Y. Li, *Energy Environ. Sci.* **2014**, 7(7), 2160–2181.
- [5] X. Wu, J. J. Hong, W. Shin, L. Ma, T. Liu, X. Bi, Y. Yuan, Y. Qi, T. W. Surta, W. Huang, J. Neuefeind, T. Wu, P. A. Greaney, J. Lu, X. Ji, *Nat. Energy* **2019**, 4(2), 123–130.
- [6] C. Lu, X. Chen, *Nano Lett* **2020**, 20(3), 1907–1914.
- [7] F. Yue, Z. Tie, S. Deng, S. Wang, M. Yang, Z. Niu, *Angew Chem Int Ed Engl* **2021**, 60(25), 13882–13886.
- [8] W. Sun, Z. Xu, C. Qiao, B. Lv, L. Gai, X. Ji, H. Jiang, L. Liu, *Adv Sci (Weinh)* **2022**, 9(27), e2201679.
- [9] N. Sun, F. Lu, Y. Yu, L. Su, X. Gao, L. Zheng, *ACS Appl Mater Interfaces* **2020**, 12(10), 11778–11788.
- [10] J. A. Wang, Y. T. Lu, S. C. Lin, Y. S. Wang, C. M. Ma, C. C. Hu, *ACS Appl Mater Interfaces* **2018**, 10(21), 17871–17882.
- [11] Z. Wang, Q. Pan, *Adv. Funct. Mater.* **2017**, 27(24), 1700690.
- [12] Y. Zhang, H. Qin, M. Alfred, H. Ke, Y. Cai, Q. Wang, F. Huang, B. Liu, P. Lv, Q. Wei, *Energy Storage Mater.* **2021**, 42, 88–96.
- [13] S. Huang, L. Hou, T. Li, Y. Jiao, P. Wu, *Adv Mater* **2022**, 34(14), e2110140.
- [14] X. F. Zhang, X. Ma, T. Hou, K. Guo, J. Yin, Z. Wang, L. Shu, M. He, J. Yao, *Angew Chem Int Ed Engl* **2019**, 58(22), 7366–7370.
- [15] G. Yang, J. Huang, X. Wan, B. Liu, Y. Zhu, J. Wang, O. Fontaine, S. Luo, P. Hiralal, Y. Guo, H. Zhou, *EcoMat* **2022**, 4(2), e12165.
- [16] X. P. Morelle, W. R. Illeperuma, K. Tian, R. Bai, Z. Suo, J. J. Vlassak, *Adv Mater* **2018**, 30(35), e1801541.
- [17] Sui, X.; Guo, H.; Cai, C.; Li, Q.; Wen, C.; Zhang, X.; Wang, X.; Yang, J.; Zhang, L, *Chemical Engineering Journal* **2021**, 419, 129478.
- [18] F. Hofmeister, *Arch. Exp. Path. Pharm.* **1888**, 24, 247–260.

- [19] W. Kunz, J. Henle, B. W. Ninham, *Curr. Opin. Colloid Interface Sci.* **2004**, 9(1–2), 19–37.
- [20] S. Furyk, Y. Zhang, D. E. Bergbreiter, P. S. Cremer, *JAM. CHEM. SOC.* **2005**, 127, 14505–14510.
- [21] Y. Zhang, P. S. Cremer, *Curr Opin Chem Biol* **2006**, 10(6), 658–663.
- [22] B. Luo, C. Cai, T. Liu, X. Meng, X. Zhuang, Y. Liu, C. Gao, M. Chi, S. Zhang, J. Wang, Y. Bai, S. Wang, S. Nie, *Adv. Funct. Mater.* **2023**, 33(42), 2306810.
- [23] H. Muta, M. Miwa, M. Satoh, *Polymer* **2001**, 42, 6313–6316.
- [24] P. Jungwirth, P. S. Cremer, *Nat Chem* **2014**, 6(4), 261–263.
- [25] R. S. Carnegie, C. L. Gibb, B. C. Gibb, *Angew Chem Int Ed Engl* **2014**, 53(43), 11498–11500.
- [26] M. Jaspers, A. E. Rowan, P. H. J. Kouwer, *Adv. Funct. Mater.* **2015**, 25(41), 6503–6510.
- [27] Y. Wu, J. Qu, X. Zhang, K. Ao, Z. Zhou, Z. Zheng, Y. Mu, X. Wu, Y. Luo, S. P. Feng, *ACS Nano* **2021**, 15(8), 13427–13435.
- [28] Q. He, Y. Huang, S. Wang, *Adv. Funct. Mater.* **2017**, 28(5), 1705069.
- [29] S. Wu, M. Hua, Y. Alsaad, Y. Du, Y. Ma, Y. Zhao, C. Y. Lo, C. Wang, D. Wu, B. Yao, J. Strzalka, H. Zhou, X. Zhu, X. He, *Adv Mater* **2021**, 33(11), e2007829.
- [30] W. Cui, Y. Zheng, R. Zhu, Q. Mu, X. Wang, Z. Wang, S. Liu, M. Li, R. Ran, *Adv. Funct. Mater.* **2022**, 32(39), 2204823.
- [31] D. Reber, R. Grissa, M. Becker, R. S. Kühnel, C. Battaglia, *Adv. Energy Mater.* **2020**, 11(5), 2002913.
- [32] M. H. Lee, S. J. Kim, D. Chang, J. Kim, S. Moon, K. Oh, K.-Y. Park, W. M. Seong, H. Park, G. Kwon, B. Lee, K. Kang, *Mater. Today* **2019**, 29, 26–36.
- [33] Y. Yuan, J. Yang, Z. Liu, R. Tan, M. Chuai, J. Sun, Y. Xu, X. Zheng, M. Wang, T. Ahmad, N. Chen, Z. Zhu, K. Li, W. Chen, *Adv. Energy Mater.* **2022**, 12(16), 2103705.
- [34] M. Qiu, P. Sun, K. Han, Z. Pang, J. Du, J. Li, J. Chen, Z. L. Wang, W. Mai, *Nat Commun* **2023**, 14(1), 601.
- [35] C. Yan, Y. Wang, X. Deng, Y. Xu, *Nanomicro Lett* **2022**, 14(1), 98.
- [36] Y. Wu, Y. Mu, Y. Luo, C. Menon, Z. Zhou, P. K. Chu, S. P. Feng, *Adv. Funct. Mater.* **2021**, 32(15), 2110859.
- [37] C. Tiyaniboonchaiya, J. M. Pringle, J. Sun, N. Byrne, P. C. Howlett, D. R. MacFarlane, M. Forsyth, *Nat Mater* **2004**, 3(1), 29–32.
- [38] K. Leng, G. Li, J. Guo, X. Zhang, A. Wang, X. Liu, J. Luo, *Adv. Funct. Mater.* **2020**, 30(23), 2001317.
- [39] C. Wang, X. Zeng, J. Qu, J. M. Cairney, Q. Meng, P. J. Cullen, Z. Pei, *Matter* **2023**, 6(11), 3993–4012.
- [40] L. Liu, X. Wu, T. Li, *J. Power Sources* **2014**, 249, 397–404.
- [41] T. Zhou, X. Gao, B. Dong, N. Sun, L. Zheng, *J. Mater. Chem. A* **2016**, 4(3), 1112–1118.
- [42] X. Peng, H. Liu, Q. Yin, J. Wu, P. Chen, G. Zhang, G. Liu, C. Wu, Y. Xie, *Nat Commun* **2016**, 7, 11782.
- [43] J. Yang, Z. Xu, J. Wang, L. Gai, X. Ji, H. Jiang, L. Liu, *Adv. Funct. Mater.* **2021**, 31(18), 2009438.
- [44] F. Mo, Z. Chen, G. Liang, D. Wang, Y. Zhao, H. Li, B. Dong, C. Zhi, *Adv. Energy Mater.* **2020**, 10(16), 2000035.
- [45] X. Yao, S. Zhang, L. Qian, N. Wei, V. Nicu, S. Coseri, F. Han, *Adv. Funct. Mater.* **2022**, 32(33), 2204565.
- [46] K. Gong, L. Hou, P. Wu, *Adv Mater* **2022**, 34(19), e2201065.
- [47] E. R. Nightingale, *J. Phys. Chem.* **1959**, 63(9), 1381–1387.
- [48] Y. H. Zhang, C. K. Chan, *J. Phys. Chem. A* **2003**, 107, 5956–5962.
- [49] Q. Zhang, Y. Ma, Y. Lu, L. Li, F. Wan, K. Zhang, J. Chen, *Nat Commun* **2020**, 11(1), 4463.

Manuscript received: April 9, 2024

Revised manuscript received: July 10, 2024

Accepted manuscript online: July 17, 2024

Version of record online: September 5, 2024